Integrated nanoplasmonic quantum interfaces for room-temperature single-photon sources

Integrated nanoplasmonic quantum interfaces for room-temperature single-photon sources

Frédéric Peyskens*
Quantum Photonics Group, RLE, Massachusetts Institute of Technology, Cambridge, Massachusetts 02139, USA

Darrick Chang
ICFO-Institut de Ciencies Fotoniques, The Barcelona Institute of Science and Technology, 08860 Castelldefels, Barcelona, Spain

Dirk Englund
Quantum Photonics Group, RLE, Massachusetts Institute of Technology, Cambridge, Massachusetts 02139, USA

(Received 10 September 2017; revised manuscript received 9 November 2017; published 29 December 2017; corrected 5 January 2018)

We describe a general analytical framework of a nanoplasmonic cavity-emitter system interacting with a dielectric photonic waveguide. Taking into account emitter quenching and dephasing, our model directly reveals the single-photon extraction efficiency η as well as the indistinguishability I of photons coupled into the waveguide mode. Rather than minimizing the cavity modal volume, our analysis predicts an optimum modal volume to maximize η that balances waveguide coupling and spontaneous emission rate enhancement. Surprisingly, our model predicts that near-unity indistinguishability is possible, but this requires a much smaller modal volume, implying a fundamental performance trade-off between high η and I at room temperature. Finally, we show that maximizing ηI requires that the system has to be driven in the weak coupling regime because quenching effects and decreased waveguide coupling drastically reduce η in the strong coupling regime.

DOI: 10.1103/PhysRevB.96.235151

I. INTRODUCTION

Atomic and photonic quantum systems are central in many areas of quantum information processing, including quantum computing, communication, and precision sensing [1–3]. A central remaining challenge is to improve the naturally weak interaction between single photons and single emitters [4]. To this end, a plethora of approaches using dielectric [5–13] as well as plasmonic [14–21] cavities and waveguides has been suggested. While several theoretical studies analyzed the interaction between quantum emitters and dielectric [4,22–25] or plasmonic [14–16] waveguides, it has been a remaining issue to develop a comprehensive physical model of a nanoplasmonic cavity interacting with a single quantum emitter and evanescently coupled to a dielectric waveguide [26,27]. A distinct advantage of such plasmonic cavities over dielectric cavities is their bandwidth. In order to achieve sufficiently large Purcell factors, dielectric cavities require large quality factors due to their diffraction limited modal volumes. This imposes stringent requirements on the cavity tuning and scalability. Moreover, the high quality factors imply slow response times [26]. Plasmonic antennas, on the other hand, can compete with free space dielectric based single-photon sources in terms of brightness and timing performance because, even for slow emitters, picosecond lifetimes can be reached due to their huge Purcell factors over a large bandwidth. It is however a remaining question how the efficiency of such plasmonic systems can be improved, especially in the context of integrated systems because most record performances have been reported for radiation into free space. Additionally, it is an open question which amount of indistinguishability can be reached with such systems [26]. As such, there is a need for a comprehensive theoretical model to analyze the single-photon extraction efficiency and indistinguishability of integrated nanoplasmonic systems, to assess their ultimate performance compared to dielectric systems.

In this paper we present a general theory framework of an integrated nanoplasmonic quantum interface which incorporates the impact of quenching and dephasing on the single-photon extraction efficiency η and indistinguishability I. Our analysis yields optimal operating conditions to maximize η and I and gives clear physical intuition in the fundamental performance trade-offs. We reveal that η is maximized for an optimum cavity modal volume V_η^{opt} which is inversely proportional to the cavity Q factor. On the other hand, I can only be maximized for much smaller $V_c \ll V_\eta^{\text{opt}}$ at room temperature, imposing a fundamental limit on the ηI product. Finally, it is shown that the maximum ηI product is obtained for weak coupling because quenching effects and reduced waveguide coupling induce a huge decrease of η in the strong coupling regime.

II. MODEL

The quantum photonic platform under investigation is shown in Fig. 1. It consists of a dielectric nanophotonic waveguide that evanescently interacts with a cavity-emitter system. The cavity has a resonance frequency ω_c and an overall linewidth $\gamma_p = \gamma_c + \kappa$, including the intrinsic linewidth γ_c and the coupling rate κ between the cavity mode (characterized by the operator p, annihilating a cavity excitation) and the waveguide mode $\gamma_c = \omega_c/(2Q) = \gamma_{\text{rad}} + \gamma_{\text{abs}}$, with γ_{rad} the radiative decay rate to the nonguided modes, γ_{abs} the absorption decay rate, and Q the unloaded quality factor. The two-level quantum emitter has a resonance frequency ω_e between its ground $|g\rangle$ and excited $|e\rangle$ state ($S_z = 1/2(|e\rangle\langle e| - |g\rangle\langle g|)$, $S_+ = |e\rangle\langle g|$, $S_- = |g\rangle\langle e|$) and a decay rate γ_e. The emitter and cavity couple at a rate Ω. We also allow for pure dephasing at a rate γ^*, which at room temperature can be orders of magnitude larger than γ_e [28].

*fpeysken@mit.edu

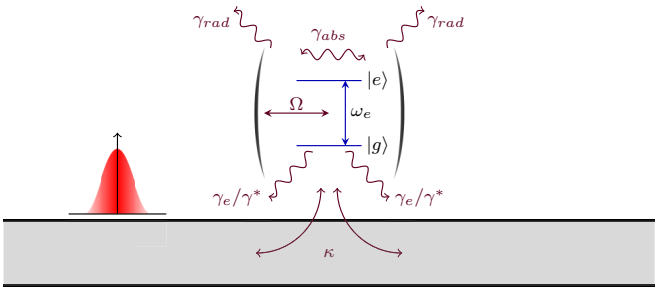

FIG. 1. Quantum photonic platform. The waveguide (gray) supports a 1D continuum of modes and interacts evanescently with a cavity-emitter system. All coupling rates and frequencies are explained in the main text. A short excitation pulse (red) through the waveguide is used to initialize the system into $|e,0\rangle$.

We model the combined dissipative quantum system using a master equation in a frame rotating at ω_e (see the Supplemental Material [29]),

$$\begin{aligned}\frac{d\rho}{dt} &= -\frac{i}{\hbar}[\mathcal{H}_{\rm rot},\rho] + \frac{\gamma_p}{2}(2p\rho p^\dagger - p^\dagger p\rho - \rho p^\dagger p)\\ &+ \frac{\gamma_e}{2}(2S_-\rho S_+ - S_+S_-\rho - \rho S_+S_-)\\ &+ \frac{\gamma^*}{2}(2S_z\rho S_z - S_zS_z\rho - \rho S_zS_z), \end{aligned} \tag{1}$$

where $\mathcal{H}_{\rm rot} = \hbar\delta_c p^\dagger p + \hbar\Omega(pS_+ + p^\dagger S_-)$ with $\delta_c = \omega_c - \omega_e$. We assume that a short excitation pulse initializes the atomic emitter into the excited state $|e\rangle$ and subsequently observe the coupling back into the waveguide. The system dynamics can then be described in a Hilbert space consisting of three states: $\{|g,0\rangle, |g,1\rangle, |e,0\rangle\}$, respectively, corresponding to the atom in the ground state and no photon in the cavity, the atom in the ground state and one photon in the cavity, or the atom in the excited state and no photon in the cavity. Moreover, we assume the nanoplasmonic cavity is a metallic spherical nanoparticle with radius R because Ω and γ_e can be calculated analytically for this specific case. More specifically, we will show below that these master equation parameters can be correlated with the parameters obtained for dipole emission near a spherical metallic nanoparticle when the emitter is expected to decay exponentially and obeys Fermi's golden rule (which is then used to calculate the overall emitter decay rate $\gamma_{\rm tot}$). The overall decay rate $\gamma_{\rm tot}$ consists of a radiative and nonradiative contribution. For an emitter in a background medium with relative permittivity ϵ_d (refractive index n_d) and near a nanoplasmonic cavity, the radiative part contains both free-space emission ($\approx\gamma_d = \gamma_0\sqrt{\epsilon_d} = \gamma_0 n_d$) as well as cavity-mediated radiation ($\gamma^c_{\rm rad}$), while the nonradiative part ($\gamma^c_{\rm nrad}$) describes the quenching effect near a metallic nanoparticle (which is absent for dielectric cavities). So $\gamma_{\rm tot} = \gamma_d + \gamma^c_{\rm rad} + \gamma^c_{\rm nrad}$. If the emitter is positioned at a distance d from the spherical metallic surface one can calculate $\gamma^c_{\rm nrad}$ in the electrostatic approximation by a multipole expansion of the coupling to the plasmon modes [20],

$$\gamma^c_{\rm nrad} = \sum_{l=1}^{\infty}\Omega_1^2\left(\frac{(2l+1)(l+1)^2}{12l(1+\xi)^{2l-2}}\right)\left(\frac{\frac{\gamma_i}{2}}{(\omega-\omega_l)^2+\left(\frac{\gamma_i}{2}\right)^2}\right), \tag{2}$$

with $\xi = d/R$, $\Omega_1^2 = \frac{9c^3\gamma_0}{\omega_p^2R^3(1+\xi)^6} = \frac{9\pi c^3\gamma_0}{\epsilon_d\omega_p^2(1+\xi)^6}(\frac{1}{V_c})$ the coupling constant to the dipole mode ($l=1$), with V_c the cavity modal volume, and $\omega_l = \omega_p\sqrt{\frac{l}{l\epsilon_\infty+(l+1)\epsilon_d}}$ the resonance frequencies of the plasmon modes. Moreover, ω_p is the plasma frequency of the metal and γ_i the intrinsic metal absorption loss as determined by the Drude model $\epsilon_M = \epsilon_\infty - \frac{\omega_p^2}{\omega^2+i\omega\gamma_i}$.

In order to explicitly incorporate the effect of the plasmon modes into our quantum master equation we start from the assumption that the atomic resonance lines up with the fundamental dipole mode, i.e., $\omega_e = \omega_1$. Any emission (both radiative and nonradiative) mediated by the $l=1$ mode will be treated through the Jaynes-Cummings terms associated with the cavity. As such, the term $\hbar\Omega(pS_+ + p^\dagger S_-)$ describes the coupling between the emitter and the fundamental $l=1$ mode ($\omega_c = \omega_1$) while γ_c contains the radiative ($\gamma_{\rm rad}$) and nonradiative ($\gamma_{\rm abs}$) decay through the $l=1$ cavity mode. The goal is now to correlate the Jaynes-Cummings parameters (Ω and γ_c) to the parameters in the $l=1$ contribution of $\gamma_{\rm tot}$. To this end, we first consider the nonradiative decay of a general quantum state $|\psi(t)\rangle = c_g(t)|g,1\rangle + c_e(t)|e,0\rangle$ consisting of either the emitter in the ground state and one photon in the cavity or the emitter in the excited state and no photon in the cavity. If we only consider nonradiative decay (which for $l=1$ is mediated by $\gamma_{\rm abs}$), the Schrödinger equations for $c_g(t)$ and $c_e(t)$, respectively, reduce to $\frac{dc_g(t)}{dt} = -i\Omega c_e(t) - (i\delta_c + \frac{\gamma_{\rm abs}}{2})c_g(t)$, $\frac{dc_e(t)}{dt} = -i\Omega c_g(t)$, with $\delta_c = \omega - \omega_1$. For sufficiently small Ω, one can adiabatically eliminate $c_g(t)$ by setting $\frac{dc_g(t)}{dt} = 0$, which eventually results in $\frac{dc_e(t)}{dt} = -\frac{\Omega^2}{i\delta_c+\frac{\gamma_{\rm abs}}{2}}c_e(t)$. The absorption mediated decay rate of the excited state emitter $|e,0\rangle$ due to the $l=1$ mode is then determined by $\frac{d|c_e(t)|^2/dt}{|c_e(t)|^2} = -\frac{\Omega^2\gamma_{\rm abs}}{\delta_c^2+(\frac{\gamma_{\rm abs}}{2})^2}$. The latter decay rate should now be identified with the $l=1$ contribution of $\gamma^c_{\rm nrad}$, i.e., $\Omega_1^2(\frac{\frac{\gamma_i}{2}}{(\omega-\omega_1)^2+(\frac{\gamma_i}{2})^2}) \equiv \frac{\Omega^2\gamma_{\rm abs}}{\delta_c^2+(\frac{\gamma_{\rm abs}}{2})^2}$. Since $\delta_c = \omega - \omega_1$, we can identify $\gamma_{\rm abs} = \gamma_i$ and $\Omega = \frac{\Omega_1}{\sqrt{2}}$. At optical frequencies the Drude model parameters of gold are $\omega_p = 14\times10^3$ THz, $\epsilon_\infty = 9$, $\gamma_i = 100$ THz [30], implying an absorption Q factor of $Q \approx 15$. For small particles the huge $\gamma_{\rm abs}$ will usually dominate over $\gamma_{\rm rad}$, meaning that the overall cavity decay rate $\gamma_c \approx \gamma_{\rm abs} = \gamma_i$ can be well approximated by a single Q factor of $Q \approx 15$ for visible frequencies, i.e., $\gamma_c \approx \frac{\omega_c}{2Q}$ with $\omega_c \approx 2957$ THz (637 nm).

Now we only need to determine the effective decay rate γ_e, which incorporates emission into all channels other than the $l=1$ cavity mode. Since the atom is off-resonant with the higher order modes one can neglect strong coupling effects with these modes. In that case we can adiabatically eliminate the higher order modes ($l>1$) and incorporate them into this effective decay rate (i.e., a local density of states). If the spherical particle is small enough (i.e., $R \ll \lambda$), the dipolar mode ($l=1$) will be the only one with nonvanishing dipole moment [31]. Therefore it is reasonable to assume that the dipole mode is the only one that will significantly contribute to $\gamma^c_{\rm rad}$, so apart from the intrinsic decay rate γ_d, the effective decay rate γ_e hence contains the nonradiative part of all higher order modes ($l>1$), i.e., $\gamma_e = \gamma_d + \frac{\Omega_1^2}{2}f_q = \gamma_d + \Omega^2 f_q$,

with

$$f_q = \sum_{l=2}^{\infty} \left(\frac{(2l+1)(l+1)^2}{12l(1+\xi)^{2l-2}} \right) \left(\frac{\gamma_c}{(\omega_e - \omega_l)^2 + \left(\frac{\gamma_c}{2}\right)^2} \right), \quad (3)$$

where we used the fact that the master equation is evaluated in a frame rotating at $\omega = \omega_e$ and that $\gamma_i = \gamma_{\text{abs}} \approx \gamma_c$. Now we have fully expressed the parameters appearing in the quantum master equation (i.e., $\Omega, \gamma_c, \gamma_e$) in terms of the parameters for dipole emission near a spherical metallic nanoparticle.

The only remaining parameter in the master equation is κ, which can be derived by noting that the plasmonic mode has a dipole moment $\mathbf{d}_c$ associated with the specific charge distribution $\rho(\mathbf{r})$ of the mode, i.e., $\mathbf{d}_c(\mathbf{r}_c) = \iiint \rho(\mathbf{r})[\mathbf{r} - \mathbf{r}_c]d\mathbf{r} \triangleq \alpha_p \mathbf{E}_c(\mathbf{r}_c)$, where we have introduced the plasmon polarizability α_p relating $\mathbf{d}_c(\mathbf{r}_c)$ to the cavity field $\mathbf{E}_c(\mathbf{r}_c)$ (both evaluated at the center of the antenna $\mathbf{r}_c$). Dot multiplying the above equation with $\overline{\mathbf{E}}_c(\mathbf{r}_c)$ eventually results in $\alpha_p = \epsilon_0 \left(\frac{\epsilon_d \overline{\mathbf{E}}_c(\mathbf{r}_c) \cdot [\iiint \nabla \cdot \mathbf{D}_r(\mathbf{r})[\mathbf{r} - \mathbf{r}_c]d\mathbf{r}]}{\iiint d\mathbf{r} \epsilon(\mathbf{r}) |E_c(\mathbf{r})|^2} \frac{|\mathbf{E}_c^m|^2}{|\mathbf{E}_c(\mathbf{r}_c)|^2} \right) V_c$, implying $\alpha_p = \epsilon_0 \alpha_0 V_c$, where $V_c = \frac{\iiint d\mathbf{r} \epsilon(\mathbf{r}) |E_c(\mathbf{r})|^2}{\epsilon_d |\mathbf{E}_c^m|^2}$ is the cavity modal volume defined using the maximum cavity electric field strength $|\mathbf{E}_c^m|$ (obtained in a region with relative dielectric permittivity ϵ_d). Moreover we factored out ϵ_0 such that the dielectric displacement is calculated using the relative permittivities $[\mathbf{D}_r(\mathbf{r})]$. The interaction between the waveguide mode and the dipole moment of the plasmonic cavity is $-\mathbf{d}_c(\mathbf{r}_c) \cdot \mathbf{E}_{\text{wg}}(\mathbf{r}_c) = -\alpha_p \mathbf{E}_c(\mathbf{r}_c) \cdot \mathbf{E}_{\text{wg}}(\mathbf{r}_c)$, where $\mathbf{E}_{\text{wg}}(\mathbf{r}_c)$ is the strength of the evanescent modal field of the waveguide. After normalization of the electric fields associated with the waveguide mode and the plasmon mode we can then derive the coupling constant $g_{\text{wg}} = \frac{\alpha_p}{\hbar} \sqrt{\frac{L}{2\pi}} \left(\sqrt{\frac{\hbar \omega_c |\mathbf{E}_c(\mathbf{r}_c)|^2}{2 \iiint_{V_c} d\mathbf{r} \epsilon_0 \epsilon(\mathbf{r}) |\mathbf{E}_c(\mathbf{r})|^2}} \right) \times \left(\sqrt{\frac{\hbar \omega_c |\mathbf{E}_{\text{wg}}(\mathbf{r}_c)|^2}{2L \iint d\mathbf{r} \epsilon_0 \epsilon(\mathbf{r}) |\mathbf{E}_{\text{wg}}(\mathbf{r})|^2}} \right) (\mathbf{u}_c \cdot \mathbf{u}_{\text{wg}})^2$. The length L is an arbitrary length along the propagation direction and arises due to the transition from a discrete number of modes to a mode continuum [24], but cancels out after normalization [32]. The unit vectors $\mathbf{u}_c$ and $\mathbf{u}_{\text{wg}}$ define the polarization of the plasmon mode and waveguide mode, respectively. The decay rate between the waveguide mode and the plasmonic cavity is then eventually $\kappa = \frac{4\pi g_{\text{wg}}^2}{c} = \frac{\alpha_p^2 \omega_c^2}{2c\epsilon_0^2 \epsilon_d \epsilon_{\text{wg}}} \left(\frac{1}{V_c} \right) \left(\frac{1}{A_{\text{eff}}} \right) \chi^{\kappa}$, where $A_{\text{eff}} = \frac{\iint d\mathbf{r} \epsilon(\mathbf{r}) |\mathbf{E}_{\text{wg}}(\mathbf{r})|^2}{\epsilon_{\text{wg}} |\mathbf{E}_{\text{wg}}^m|^2}$ is the effective modal area of the waveguide mode, $|\mathbf{E}_{\text{wg}}^m|$ is the maximum electric field strength of the waveguide mode (obtained in a region with relative dielectric permittivity ϵ_{wg}), and $\chi^{\kappa} = \frac{|\mathbf{E}_{\text{wg}}(\mathbf{r}_c)|^2}{|\mathbf{E}_{\text{wg}}^m|^2} \frac{|\mathbf{E}_c(\mathbf{r}_c)|^2}{|\mathbf{E}_c^m|^2} (\mathbf{u}_c \cdot \mathbf{u}_{\text{wg}})^2$ is a factor incorporating the overlap between the waveguide and cavity mode. Finally one gets

$$\kappa = \frac{\omega_c^2 \chi^{\kappa}}{2cA_{\text{eff}} \epsilon_d \epsilon_{\text{wg}}} \left(\frac{\alpha_0^2 V_c^2}{V_c} \right) = \frac{\omega_c^2 \chi^{\kappa} \alpha_0^2 V_c}{2cA_{\text{eff}} \epsilon_d \epsilon_{\text{wg}}}. \quad (4)$$

The effective modal area A_{eff} can also be expressed as a function of the effective mode index $n_{\text{eff}} = \sqrt{\epsilon_{\text{eff}}}$, $A_{\text{eff}} \approx \left(\frac{\lambda_c}{2n_{\text{eff}}} \right)^2$ [33]. For a spherical particle in a background medium with relative permittivity ϵ_d, the dipole moment of the fundamental plasmon mode is $\mathbf{d} = 2\epsilon_0 \epsilon_d V_c \mathbf{E} = \alpha_p \mathbf{E}$, i.e., $\alpha_0 = 2\epsilon_d$ [31]), such that $\kappa = \frac{\omega_c^4 \alpha_0^2 \chi^{\kappa} \epsilon_{\text{eff}}}{2\pi^2 c^3 \epsilon_d \epsilon_{\text{wg}}} V_c = \frac{2\chi^{\kappa} R^3 \omega_c^4 \epsilon_{\text{eff}}}{\pi c^3 \epsilon_{\text{wg}}}$.

III. ON-CHIP SINGLE-PHOTON GENERATION

A. Efficiency

The efficiency of emitting a single photon into the waveguide η is calculated from the time-averaged number of intracavity photons multiplied by their decay rate into the waveguide, i.e., $\eta = \kappa \int_0^{\infty} dt \langle p^{\dagger}(t) p(t) \rangle = \kappa \int_0^{\infty} dt \langle g, 1 | \rho(t) | g, 1 \rangle$. The solution of the time-dependent master equation, with $\delta_c = 0$ and the initial state of the system in $|e, 0\rangle$, can be found analytically,

$$\eta \approx \frac{\kappa}{(\gamma_e + \gamma_p)\left(1 + \frac{\gamma_e \gamma_p}{4\Omega^2}\right)}, \quad (5)$$

and is independent of the dephasing rate γ^* since $\gamma_p \gg \gamma^*$ for a nanoplasmonic cavity (see Ref. [29]).

The analytical formulas for κ, Ω, and γ_e now allow us to evaluate η as a function of ξ and R. As seen in Fig. 2(a), there exists an optimum ξ and R that maximizes η (marked by the red dot). This optimum can be understood from the limiting cases for η. Figure 2(b) plots the ratio between the loaded cavity decay rate γ_p and the total emitter linewidth, which we define here as $\theta_1 = \gamma_p / (\gamma_e + \gamma^*)$. θ_1 distinguishes the bad cavity regime ($\theta_1 \gg 1$) from the good cavity regime ($\theta_1 \ll 1$), following Ref. [28]. Comparing Figs. 2(a) and 2(b) show that the parameters for optimal η clearly fall into the bad cavity limit for which $\eta \approx [(1 + \frac{\gamma_c}{\kappa})(1 + \frac{\gamma_e(\kappa + \gamma_c)}{4\Omega^2})]^{-1}$. Since $\gamma_e = \gamma_d + \Omega^2 f_q$ is an explicit function of Ω, two limiting cases emerge. Either η is limited by the intrinsic decay rate, i.e., $\gamma_e \approx \gamma_d$, or by quenching, i.e., $\gamma_e \approx \Omega^2 f_q$ [see the plot of γ_e / γ_d in Fig. 2(c)]. For large $\xi > 10$, the quenching factor $f_q \propto \xi^{-2}$ approaches zero and any increase in ξ only reduces Ω, implying a concomitant decrease in η. On the other hand, if $\xi \to 0$, $f_q \propto \xi^{-3}$, eventually reducing the single-photon emission as well. As such the optimum ξ_{opt} is expected at the crossover region between the intrinsic decay rate limited and quenching limited case [which is confirmed by Fig. 2(c)]. The optimum in R strikes a balance between an increased cavity-emitter coupling strength $\Omega^2 \propto 1/V_c$ due to the confinement of the cavity photon to a small modal volume, and a simultaneous reduction in the radiative emission rate $\kappa \propto V_c$ due to the smaller dipole moment. While one desires an out-coupling to the waveguide mode κ which is as large as possible, a continuous increase in R (V_c) also reduces Ω, eventually reducing η again. In the Supplemental Material [29] it is shown that for ξ values in the crossover region, the optimal cavity modal volume is approximately given by

$$V_{\eta}^{\text{opt}} \approx \frac{\lambda_c^3}{Q} \left(\frac{\epsilon_d \epsilon_{\text{wg}}}{8\pi \chi^{\kappa} \alpha_0^2 \epsilon_{\text{eff}}} \right). \quad (6)$$

The optimum cavity modal volume hence has to increase if either the Q factor, the cavity polarizability, or the overlap between the cavity and the waveguide mode is reduced. Similarly, if the effective modal area increases (i.e., lower ϵ_{eff}), the waveguide mode becomes less confined and will spread out over a larger area in the vicinity of the waveguide core. Consequently, the evanescent coupling with nearby cavity-emitter systems will decrease, again necessitating an increase in V_c. This result clearly demonstrates that it is not always beneficial to achieve the smallest possible modal volume and hence

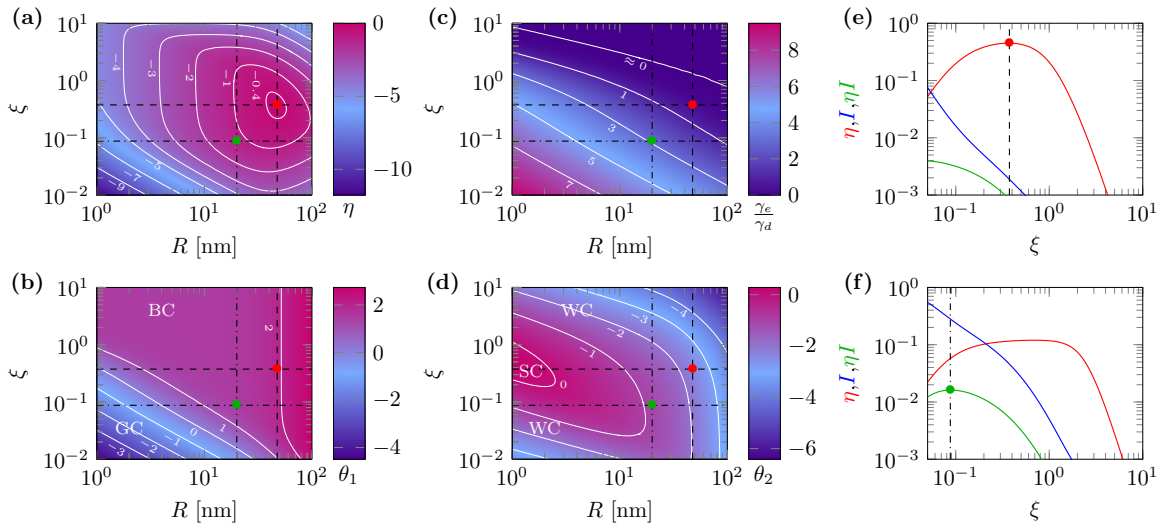

FIG. 2. Single-photon characteristics ($\lambda_c = 637$ nm) for a nanoplasmonic cavity with $Q = 15$, $\gamma_d = 1$ GHz, $\gamma^* = 3.5$ THz (a realistic value at room temperature [28]); $\epsilon_{\text{eff}} = 4$ and $\epsilon_{\text{wg}} = 4$ (realistic values for a silicon nitride waveguide); $\chi^\kappa = 1$ (in practice $\chi^\kappa < 1$ due to an imperfect overlap between the cavity and the waveguide; as such the obtained values are the theoretical upper limits). Moreover, 1000 higher-order modes are incorporated to guarantee convergence. (a) Single-photon extraction efficiency η. (b) $\theta_1 = \gamma_p/(\gamma_e + \gamma^*)$ defining the bad ($\theta_1 \gg 1$, BC) and good ($\theta_1 \ll 1$, GC) cavity limit. (c) γ_e/γ_d ratio to assess the quenching strength. (d) $\theta_2 = 2\Omega/(\gamma_e + \gamma_p + \gamma^*)$ defining the regions of strong ($\theta_2 \gg 1$, SC) and weak ($\theta_2 \ll 1$, WC) coupling. All surface plots are on a $\log_{10}$ scale. (e) and (f) η (red), I (blue), and ηI (green) for two R slices: (e) $R = 47.5$ nm [vertical dashed line in (a)–(d)] and (f) $R = 20$ nm [vertical dash-dotted line in (a)–(d)]. The intersection between either the vertical and horizontal dashed (red circle) or dash-dotted (green circle) lines in (a)–(d), respectively, marks the maximum of η in (e) and the maximum of ηI in (f).

serves as an important caveat to the commonly used strategy of reducing it to increase cavity-emitter interactions. In particular, while the interaction strength does increase for smaller V_c, such a strength is not helpful if the information contained in the cavity photon cannot escape into the waveguide.

B. Indistinguishability

Apart from generating single photons with high efficiency, many applications require the photons to be indistinguishable. Therefore, we also investigate the indistinguishability I of two photons emitted by an integrated nanoplasmonic cavity. Depending on the previously defined ratio θ_1 and the ratio $\theta_2 = 2\Omega/(\gamma_e + \gamma_p + \gamma^*)$ [shown in Fig. 2(d)], one can distinguish three limiting cases for the indistinguishability, as introduced in Ref. [28]. From Fig. 2(d) it is clear that $\theta_2 \ll 1$ for most parameter values, meaning that our system is in the weak coupling regime. In this regime, one can either operate in the previously introduced good cavity or bad cavity limit. Achieving high I in the bad cavity limit is difficult for dielectric cavities since their coupling strengths usually cannot compensate for room-temperature dephasing [28]. On the contrary, nanoplasmonic antennas allow much larger coupling strengths, turning the bad cavity limit into a regime of practical interest. In this limit, the effect of the cavity is to add an extra channel of irreversible emission at a rate $R = 4\Omega^2/(\gamma_e + \gamma^* + \gamma_p)$, such that the dynamics of the coupled system can be described by an effective quantum emitter with decay rate $\gamma_e + R$, i.e., $I = (\gamma_e + R)/(\gamma_e + R + \gamma^*)$ [28]. Maximizing I requires the cavity modal volume to be much smaller than an upper limit V_u,

$$V_c \ll V_u = V_\eta^{\text{opt}} \left(\frac{\alpha_0}{\epsilon_d}\right)^2 \left(\frac{\epsilon_{\text{eff}}}{\epsilon_{\text{wg}}}\right) \left(\frac{\gamma_0}{\gamma^*}\right) Q^2 \chi^\kappa. \qquad (7)$$

This constraint mainly stems from the fact that the cavity-emitter coupling must be large enough to exceed the dephasing rate, necessitating very small modal volumes [29]. However, V_u is typically much smaller than the optimum modal volume for η because room-temperature γ_0/γ^* ratios are usually on the order of 10^{-3} or 10^{-4}. Our model therefore shows conflicting requirements for maximizing I and η at room temperature. This trade-off between η and I is shown in Figs. 2(e) and 2(f) where η, I, and ηI are evaluated along the ξ slice for which η [Fig. 2(e)] or ηI [Fig. 2(f)] are maximized, respectively. The (ξ, R) combination that maximizes ηI is marked by a green dot in Figs. 2(a)–2(d). Figure 2(e) shows that for the given parameters $\eta \approx 45\%$ at $\xi \approx 0.38$ and $R \approx 47.5$ nm. Nevertheless, the indistinguishability is low (≈0.2%). When considering the R slice along which ηI is maximal (≈1.6% for $R = 20$ nm and $\xi = 0.09$), η drops to ∼5.7%, while I increases to ∼28% [Fig. 2(f)]. Indeed, the increase in I is accompanied by a $(47.5/20)^3 \approx 10$-fold reduction in cavity modal volume. For sufficiently small ξ and/or R values, one can moreover achieve the good cavity or strong coupling limit [see Figs. 2(b) and 2(d)]. In both regimes it is possible to generate photons with almost perfect indistinguishability at room temperature. However, the reduction in ξ and R induces large quenching effects [Fig. 2(c)], which eventually sharply reduce the single-photon extraction efficiency [see Fig. 2(a) for η values in the good cavity or strong coupling region]; for example, $I \approx 93\%$ but $\eta \approx 0.001\%$ for $R \approx 4$ nm and $\xi \approx 0.035$. The reduction in R moreover lowers η through κ. So in any of the three limiting cases there will be a trade-off between high I and high η. For dielectric cavities, high I and high η can only be achieved simultaneously in the strong coupling regime [28]. By contrast, we have shown that the

maximum ηI performance is achieved in the bad cavity limit. This is an important observation since most recent reports focus on achieving strong coupling [34–36]. While the strong coupling regime is beneficial for obtaining high I, it is also accompanied by a strong reduction in η due to quenching and reduced waveguide coupling.

It is however possible to raise V_u to partially reconcile the different constraints on the modal volume in the bad cavity limit. Apart from maximizing the overlap between the cavity and the waveguide mode ($\chi^\kappa \to 1$), there are two other ways to improve the system. First, the waveguide geometry should be optimized to maximize the effective permittivity ϵ_{eff} ($\leqslant \epsilon_{\text{wg}}$). Second, the polarizability of the fundamental dipole mode should be increased as much as possible (i.e., $\alpha_0 \gg \epsilon_d$), for example by considering rod or bowtie antennas [37,38]. Engineered antenna geometries can also achieve larger field enhancements as compared to the spherical particle case, which in turn result in higher η or ηI. In the Supplemental Material [29] it is shown that an enhancement in the field and the polarizability by a factor 10 already allows single-photon extraction efficiencies of 80% while ηI increases to 50%. Further optimization could enable room temperature on-demand ($\eta \to 1$) or perfectly indistinguishable ($I \to 1$) single-photon sources. However, achieving both at the same time (i.e., $\eta I = 1$) appears impossible for any realistic on-chip nanoplasmonic quantum interface at room temperature due to the conflicting requirements on the modal volume. If the system is cooled down such that the dephasing rate γ^* drops, it is possible to achieve much higher ηI; a reduction of the dephasing rate to O (GHz), while keeping all other parameters the same as in Fig. 2, allows $\eta I \approx 35\%$. In the absence of dephasing, ηI eventually becomes limited by η. Recently, a near optimal single-photon source was realized using InGaAs quantum dots at 4 K, reporting efficiencies of $\eta \approx 90.74\%$ with indistinguishability $I \approx 99.56\%$, yielding $\eta I \approx 90.34\%$ [39]. As such it is clear that at low temperature the investigated nanoplasmonic platform cannot compete with state-of-the-art dielectric cavity systems. It should however be noted that the obtained $\eta I = 1.6\%$ at room temperature (assuming a perfect overlap between the cavity and the waveguide mode) is already orders of magnitude higher than what can be achieved using spectral filtering and moreover approaches earlier reported values for dielectric cavities in the good cavity regime [28]. Therefore, it is expected that realistic integrated nanoplasmonic systems could only offer an advantage over dielectric systems, for room-temperature single-photon sources provided that one can compromise on either efficiency or indistinguishability.

IV. CONCLUSION

We presented a theoretical framework for a nanoplasmonic cavity-emitter system evanescently coupled to a dielectric waveguide and investigated the impact of quenching and dephasing on the single-photon extraction efficiency η and indistinguishability I. While quenching imposes fundamental limits on both η and I, dephasing only has a considerable impact on I for an integrated nanoplasmonic cavity-emitter system. We showed there exists an optimum cavity modal volume V_η^{opt} to maximize η, which balances the coupling rate into the waveguide with the emission rate enhancement. This optimum is inversely proportional to the cavity Q factor and depends on the effective modal area of the waveguide and cavity polarizability. Unfortunately, V_η^{opt} is typically much larger than the modal volume required to maximize I. This trade-off imposes a fundamental limit on the ηI product and inhibits the perfect $\eta I = 1$ value to be obtained for most experimentally achievable nanoplasmonic systems at room temperature. While the strong coupling regime is beneficial for achieving high I, we moreover showed that the maximal ηI is obtained for weak coupling. Furthermore, we addressed strategies, such as field and cavity polarizability enhancement, to partially alleviate the ηI trade-off. Our theoretical framework captures the essential physics of integrated nanoplasmonic cavities for quantum photonic applications and identifies all the important design parameters to guide future efforts in the development of integrated single-photon sources at low and room temperature.

ACKNOWLEDGMENTS

F.P. acknowledges support from a BAEF (Belgian American Educational Foundation) and Fulbright postdoctoral fellowship. D.E.C. acknowledges support from Fundacio Privada Cellex, Spanish MINECO Severo Ochoa Programme SEV-2015-0522, MINECO Plan Nacional Grant CANS, CERCA Programme/Generalitat de Catalunya, and ERC Starting Grant FOQAL.

[1] H. Kimble, Nature (London) **453**, 1023 (2008).
[2] J. O'Brien, A. Furusawa, and J. Vučković, Nat. Photon. **3**, 687 (2009).
[3] P. Lodahl, S. Mahmoodian, and S. Stobbe, Rev. Mod. Phys. **87**, 347 (2015).
[4] A. Sipahigil, R. E. Evans, D. D. Sukachev, M. J. Burek, J. Borregaard, M. K. Bhaskar, C. T. Nguyen, J. L. Pacheco, H. A. Atikian, C. Meuwly, R. M. Camacho, F. Jelezko, E. Bielejec, H. Park, M. Lončar, and M. D. Lukin, Science **354**, 847 (2016).
[5] D. Englund, A. Faraon, I. Fushman, N. Stoltz, P. Petroff, and J. Vučković, Nature (London) **450**, 857 (2007).
[6] A. Faraon, I. Fushman, D. Englund, N. Stoltz, P. Petroff, and J. Vučković, Nat. Phys. **4**, 859 (2008).
[7] A. Rundquist, M. Bajcsy, A. Majumdar, T. Sarmiento, K. Fischer, K. G. Lagoudakis, S. Buckley, A. Y. Piggott, and J. Vučković, Phys. Rev. A **90**, 023846 (2014).
[8] K. Müller, A. Rundquist, K. A. Fischer, T. Sarmiento, K. G. Lagoudakis, Y. A. Kelaita, C. Sánchez Muñoz, E. del Valle, F. P. Laussy, and J. Vučković, Phys. Rev. Lett. **114**, 233601 (2015).
[9] C. Dory, K. A. Fischer, K. Müller, K. G. Lagoudakis, T. Sarmiento, A. Rundquist, J. L. Zhang, Y. Kelaita, N. V. Sapra, and J. Vučković, Phys. Rev. A **95**, 023804 (2017).

[10] D. Press, S. Götzinger, S. Reitzenstein, C. Hofmann, A. Löffler, M. Kamp, A. Forchel, and Y. Yamamoto, Phys. Rev. Lett. **98**, 117402 (2007).
[11] L. Li, T. Schröder, E. H. Chen, M. Walsh, I. Bayn, J. Goldstein, O. Gaathon, M. E. Trusheim, M. Lu, J. Mower, M. Cotlet, M. L. Markham, D. J. Twitchen, and D. Englund, Nat. Commun. **6**, 6173 (2015).
[12] S. L. Mouradian, T. Schröder, C. B. Poitras, L. Li, J. Goldstein, E. H. Chen, M. Walsh, J. Cardenas, M. L. Markham, D. J. Twitchen, M. Lipson, and D. Englund, Phys. Rev. X **5**, 031009 (2015).
[13] H. Choi, M. Heuck, and D. Englund, Phys. Rev. Lett. **118**, 223605 (2017).
[14] D. E. Chang, A. S. Sørensen, P. R. Hemmer, and M. D. Lukin, Phys. Rev. Lett. **97**, 053002 (2006).
[15] D. E. Chang, A. S. Sørensen, P. R. Hemmer, and M. D. Lukin, Phys. Rev. B **76**, 035420 (2007).
[16] D. Chang, A. S. Sørensen, E. A. Demler, and M. D. Lukin, Nat. Phys. **3**, 807 (2007).
[17] A. V. Akimov, A. Mukherjee, C. L. Yu, D. E. Chang, A. S. Zibrov, P. R. Hemmer, and M. D. Lukin, Nature (London) **450**, 402 (2007).
[18] E. Waks and D. Sridharan, Phys. Rev. A **82**, 043845 (2010).
[19] C. Van Vlack, P. T. Kristensen, and S. Hughes, Phys. Rev. B **85**, 075303 (2012).
[20] A. Delga, J. Feist, J. Bravo-Abad, and F. J. García-Vidal, Phys. Rev. Lett. **112**, 253601 (2014).
[21] R. Sáez-Blázquez, J. Feist, A. I. Fernández-Domínguez, and F. J. García-Vidal, Optica **4**, 1363 (2017).
[22] A. Auffèves-Garnier, C. Simon, J.-M. Gérard, and J.-P. Poizat, Phys. Rev. A **75**, 053823 (2007).
[23] K. A. Fischer, Y. A. Kelaita, N. V. Sapra, C. Dory, K. G. Lagoudakis, K. Müller, and J. Vučković, Phys. Rev. Appl. **7**, 044002 (2017).
[24] S. Fan, Ş. E. Kocabaş, and J. T. Shen, Phys. Rev. A **82**, 063821 (2010).
[25] T. Caneva, M. T. Manzoni, T. Shi, J. S. Douglas, J. I. Cirac, and D. E. Chang, New J. Phys. **17**, 113001 (2015).
[26] F. Koenderink, ACS Photon. **4**, 710 (2017).
[27] S. I. Bozhevolnyi and J. B. Khurgin, Nat. Photon. **11**, 398 (2017).
[28] T. Grange, G. Hornecker, D. Hunger, J.-P. Poizat, J.-M. Gérard, P. Senellart, and A. Auffèves, Phys. Rev. Lett. **114**, 193601 (2015).
[29] See Supplemental Material at http://link.aps.org/supplemental/10.1103/PhysRevB.96.235151 for a derivation of the master equation, the single-photon extraction efficiency, the condition for high indistinguishability, and a plot on the effect of field enhancement and improved cavity polarizability.
[30] A. Vial, A.-S. Grimault, D. Macías, D. Barchiesi, and M. L. de la Chapelle, Phys. Rev. B **71**, 085416 (2005).
[31] G. Sun, J. B. Khurgin, and A. Bratkovsky, Phys. Rev. B **84**, 045415 (2011).
[32] Y. C. Jun, R. M. Briggs, H. A. Atwater, and M. L. Brongersma, Opt. Express **17**, 7479 (2009).
[33] S. Bozhevolnyi and J. B. Khurgin, Optica **3**, 1418 (2016).
[34] K. Santhosh, O. Bitton, L. Chuntonov, and G. Haran, Nat. Commun. **7**, 11823 (2016).
[35] R. Chikkaraddy, B. de Nijs, F. Benz, S. J. Barrow, O. A. Scherman, E. Rosta, A. Demetriadou, P. Fox, O. Hess, and J. J. Baumberg, Nature (London) **535**, 127 (2016).
[36] R. Liu, Z.-K. Zhou, Y.-C. Yu, T. Zhang, H. Wang, G. Liu, Y. Wei, H. Chen, and X.-H. Wang, Phys. Rev. Lett. **118**, 237401 (2017).
[37] F. Peyskens, A. Subramanian, P. Neutens, A. Dhakal, P. Van Dorpe, N. Le Thomas, and R. Baets, Opt. Express **23**, 3088 (2015).
[38] F. Peyskens, A. Dhakal, P. Van Dorpe, N. Le Thomas, and R. Baets, ACS Photon. **1**, 102 (2016).
[39] N. Somaschi, V. Giesz, L. De Santis, J. C. Loredo, M. P. Almeida, G. Hornecker, T. Portalupi, C. A. Grange, J. Demory, C. Gómez, I. Sagnes, N. D. Lanzilotti-Kimura, A. A. Lemaítre, A. G. White, L. Lanco, and P. Senellart, Nat. Photon. **10**, 340 (2016).